


**Stripe order, impurities, and symmetry breaking in a diluted frustrated magnet**Xuecheng Ye,<sup>1</sup> Rajesh Narayanan,<sup>2</sup> and Thomas Vojta <sup>1</sup><sup>1</sup>*Department of Physics, Missouri University of Science and Technology, Rolla, Missouri 65409, USA*<sup>2</sup>*Department of Physics, Indian Institute of Technology Madras, Chennai 600036, India*

(Received 9 November 2021; accepted 23 December 2021; published 4 January 2022)

We investigate the behavior of the frustrated  $J_1$ - $J_2$  Ising model on a square lattice under the influence of random dilution and spatial anisotropies. Spinless impurities generate a random-field type disorder for the spin-density wave (stripe) order parameter. These random fields destroy the long-range stripe order in the case of spatially isotropic interactions. Combining symmetry arguments, percolation theory, and large-scale Monte Carlo simulations, we demonstrate that arbitrarily weak spatial interaction anisotropies restore the stripe phase. More specifically, the transition temperature  $T_c$  into the stripe phase depends on the interaction anisotropy  $\Delta J$  via  $T_c \sim 1/|\ln(\Delta J)|$  for small  $\Delta J$ . This logarithmic dependence implies that very weak anisotropies are sufficient to restore the transition temperature to values comparable to that of the undiluted system. We analyze the critical behavior of the emerging transition and find it to belong to the disordered two-dimensional Ising universality class, which features the clean Ising critical exponents and universal logarithmic corrections. We also discuss the generality of our results and their consequences for experiments.

DOI: [10.1103/PhysRevB.105.024201](https://doi.org/10.1103/PhysRevB.105.024201)**I. INTRODUCTION**

The influence of impurities, defects, and other types of quenched random disorder on the symmetry-broken low-temperature phases of many-particle systems and on their phase transitions is an important topic in condensed matter physics. Fundamentally, disorder effects are governed by the interplay between the symmetries of the order parameters characterizing the phase or phase transition and the symmetries of the disorder (see, e.g., Ref. [1] for a pedagogical discussion).

If the impurities respect the order parameter symmetries, they generically lead to random- $T_c$  disorder, i.e., to spatial variations in the tendency towards the symmetry-broken phase. As this disorder appears in the mass term of the order parameter field theory, it is also called random-mass disorder. The diluted ferromagnet is an example for this case because spinless impurities do not prefer a particular magnetization direction and thus do not break the spin symmetry. Random-mass disorder can influence phase transitions profoundly, e.g., by rounding first-order phase transitions [2–4] or by modifying the critical behavior of continuous ones [5]. Quantum phase transitions can feature additional disorder effects including infinite-randomness critical points [6–8], smeared phase transitions [9], and quantum Griffiths singularities [10–12] (see Refs. [13,14] for reviews).

If, on the other hand, the impurities locally break the order parameter symmetries, a stronger coupling between the disorder and the order parameter can be expected. The generic result is random-field disorder [15], i.e., randomness in the field conjugate to the order parameter in the corresponding field theory. More complicated scenarios such as random-easy-axis disorder [16–20] can occur if the impurities break the order parameter symmetries only partially. Random

fields can have more dramatic effects than random-mass disorder. In sufficiently low space dimensions ( $d \leq 2$  for discrete order parameter symmetry and  $d \leq 4$  for continuous order parameter symmetry), even weak random fields destroy the symmetry-broken phase itself via domain formation [4,15,21].

Recent years have seen renewed interest in phases that spontaneously break real-space symmetries in addition to spin, phase, or gauge symmetries, including the charge-density wave or stripe phases in cuprate superconductors [22–24], the Ising-nematic phases in the iron pnictides [25–27], as well as valence-bond solids in certain quantum magnets [28–30]. In general, impurities locally break the real-space symmetries of the associated order parameters. They thus generically lead to random-field-type disorder for such order parameters [20,31–37]. In addition to destroying the original long-range order, these random fields can also induce novel phases of matter [20,37].

A prototypical model for impurity-induced random fields is the frustrated  $J_1$ - $J_2$  Ising model on a square lattice, with ferromagnetic nearest-neighbor interactions and antiferromagnetic next-nearest-neighbor interactions. For sufficiently strong next-nearest-neighbor interactions, it features a stripe-ordered low-temperature phase. As site or bond dilution locally break the symmetry between the two equivalent stripe directions, they generate random fields for the nematic order [31,36], which destroy the stripe phase via domain formation. Interestingly, the strength of the random fields can be tuned by the repulsion between the impurities [36].

In the present paper, we revisit the diluted  $J_1$ - $J_2$  Ising model and focus on the interplay between the random-field disorder and global interaction anisotropies that may arise, e.g., from strain engineering, epitaxial growth, or the shape of crystallites or samples. We combine symmetry arguments, percolation theory and large-scale Monte Carlo simulations to

show that the stripe phase is restored by an arbitrarily weak global anisotropy (modeled, e.g., by a difference  $\Delta J$  between the horizontal and vertical interaction strengths) that explicitly breaks the symmetry between the two stripe directions. Importantly, the transition temperature  $T_c$  into the stripe phase varies with the interaction anisotropy as  $T_c \sim 1/|\ln(\Delta J)|$ . This logarithmic dependence implies that a very weak anisotropy is sufficient to suppress most random-field effects and restore the transition temperature to a value comparable to that of the undiluted system. We also determine the critical behavior of the emerging phase transition between the paramagnetic and stripe phases. Just as the transition in the diluted Ising ferromagnet, it belongs to the disordered two-dimensional Ising universality class, which is characterized by the clean Ising exponents and universal logarithmic corrections.

The remainder of our paper is organized as follows. In Sec. II, we define the  $J_1$ - $J_2$  Ising model. We also discuss the random-field mechanism and domain formation. Our computer simulation methods are introduced in Sec. III. Section IV is devoted to the simulation results and a comparison with theoretical predictions. We conclude in Sec. V by discussing the generality of our findings and their consequences for experiments.

## II. MODEL AND RANDOM-FIELD MECHANISM

### A. Diluted anisotropic $J_1$ - $J_2$ Ising model

We start with the well-known  $J_1$ - $J_2$  Ising model on a square lattice of  $N = L^2$  sites given by the Hamiltonian

$$H_0 = -J_1 \sum_{\langle ij \rangle} S_i S_j - J_2 \sum_{\langle\langle ij \rangle\rangle} S_i S_j. \quad (1)$$

Here,  $S_i = \pm 1$  is a classical Ising spin,  $\langle ij \rangle$  denotes pairs of nearest-neighbor sites coupled by the ferromagnetic interaction  $J_1 > 0$ , and  $\langle\langle ij \rangle\rangle$  denotes next-nearest-neighbor pairs coupled by the antiferromagnetic interaction  $J_2 < 0$ . The phases of this system are well-understood (see, e.g., Refs. [38–41] and references therein). It displays paramagnetic behavior at high temperatures. As the temperature is lowered, two distinct long-range ordered phases appear. For  $|J_2|/J_1 < 1/2$ , the low-temperature phase is ferromagnetic; it breaks the  $Z_2$  Ising spin symmetry but none of the real-space symmetries. For  $|J_2|/J_1 > 1/2$ , in contrast, the low-temperature phase features a stripe-like spin order that breaks not only the Ising spin symmetry but also the  $C_4$  rotation symmetry of the square lattice.

To explore the combined influence of quenched disorder and spatial anisotropies on the stripe phase, we now introduce site dilution, and we allow the nearest-neighbor interaction to take different values  $J_{1h}$  and  $J_{1v}$  for horizontal and vertical bonds, respectively (see Fig. 1). The resulting Hamiltonian reads

$$H = -J_{1h} \sum_{\langle ij \rangle_h} \epsilon_i \epsilon_j S_i S_j - J_{1v} \sum_{\langle ij \rangle_v} \epsilon_i \epsilon_j S_i S_j - J_2 \sum_{\langle\langle ij \rangle\rangle} \epsilon_i \epsilon_j S_i S_j. \quad (2)$$

The  $\epsilon_i$  are quenched random variables that can take the values 0 (representing a vacancy) with probability  $p$  and

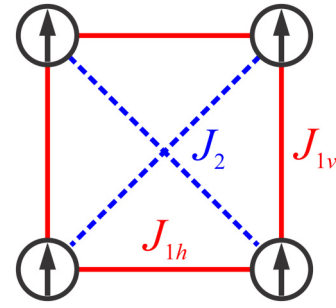


FIG. 1. Interactions of the anisotropic  $J_1$ - $J_2$  model.

1 (occupied site) with probability  $1 - p$ . We consider the  $\epsilon_i$  at different sites statistically independent; the effects of (anti)correlations between the vacancies were explored in Ref. [36]. We parametrize the nearest-neighbor interactions in terms of their average and difference,  $J_{1h} = J_1 + \Delta J$ ,  $J_{1v} = J_1 - \Delta J$ . In the following, we focus on the parameter region that favors stripe order at low temperatures, i.e., on  $|J_2|/J_1 > 1/2$ .

### B. Random-field disorder

While a single vacancy does not break the  $C_4$  rotation symmetry of the lattice, spatial arrangements of several vacancies generally do break this symmetry locally, leading to the emergence of random-field disorder that locally prefers one stripe direction over the other (even in the absence of interaction anisotropies, i.e., for  $\Delta J = 0$ ). Specifically, a pair of vacancies on horizontal nearest-neighbor sites prefers horizontal stripes by an energy difference of  $2J_1$ , see Fig. 2 [31,36]. Analogously, a vacancy pair on vertical nearest-neighbor sites prefers vertical stripes.

The typical random-field energy of a perfect (horizontal or vertical) stripe state in a system of  $L \times L$  sites can be easily estimated in the limit of low dilution  $p$  when different vacancy pairs can be considered independent and arrangements of three or more vacancies on neighboring sites are suppressed. A system of  $L \times L$  sites has  $2L^2$  distinct nearest-neighbor pairs (bonds), resulting in an average number of vacancy pairs of  $2L^2 p^2$ . The random-field energy  $E_{RF}(L)$  is thus the sum of  $2L^2 p^2$  random contributions  $\pm J_1$ . The central limit theorem then gives

$$\langle E_{RF}^2(L) \rangle = 2L^2 p^2 J_1^2 = h_{\text{eff}}^2 L^2 \quad (3)$$

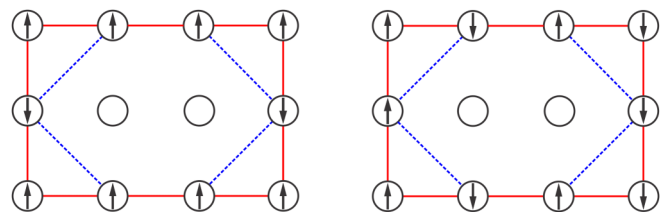


FIG. 2. Random-field mechanism: A pair of vacancies on horizontal nearest-neighbor sites prefers horizontal stripes (left) over vertical stripes (right) by an energy difference of  $2J_1$ .

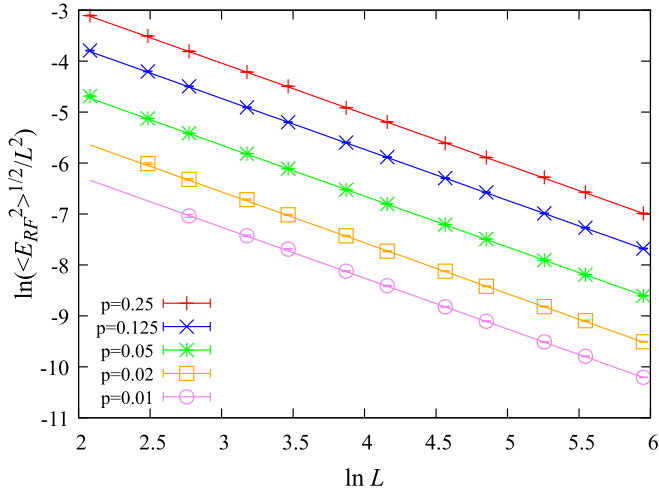


FIG. 3. Root-mean-square random-field energy of a perfect stripe state per lattice site  $\langle E_{RF}^2 \rangle^{1/2} / L^2$  vs linear system size  $L$  for several dilutions  $p$ . The data are determined by averaging the square of the energy difference between perfect horizontal and vertical stripe states over 20 000 disorder configurations. The solid lines represent relation (3) without adjustable parameters.

with effective random field strength  $h_{\text{eff}} = \sqrt{2}pJ_1$  [42]. We have confirmed the relation (3) numerically for a range of dilutions and system sizes, as can be seen in Fig. 3. It holds (at least in very good approximation) for dilutions as high as  $p = 1/4$ .

### C. Domain formation

According to Imry and Ma [15], the fate of the symmetry-broken low-temperature phase is governed by the competition between the random-field energy gain due to the formation of domains of horizontal and vertical stripes that align with the local random field and the energy cost of a domain wall. The energy cost of a straight domain wall between horizontal and vertical stripes in the undiluted  $J_1$ - $J_2$  model is easily worked out, it equals  $2|J_2|$  per lattice constant. This domain formation problem can be mapped onto a random-field Ising model with the Ising variable representing the difference between horizontal and vertical stripes in the  $J_1$ - $J_2$  model (2).

Let us first consider the case of isotropic interactions,  $\Delta J = 0$  (which maps onto an unbiased random-field Ising model). In two dimensions, domains appear for arbitrarily weak random fields beyond the so-called breakup length scale  $L_0$ . For weak random fields,  $L_0$  depends exponentially on the ratio between the domain wall energy scale  $J_2$  and the random-field strength  $h_{\text{eff}}$ ,

$$L_0 = A \exp(cJ_2^2/h_{\text{eff}}^2) \quad (4)$$

with  $A$  and  $c$  constants [21]. As horizontal and vertical stripe domains are equally likely for  $\Delta J = 0$ , the domain formation destroys the symmetry-broken low-temperature phase. (A rigorous proof that the Gibbs state in a two-dimensional random-field Ising model is unique was given by Aizenman and Wehr [4].) This agrees with the Monte Carlo simulation results of Ref. [36].

For anisotropic interactions,  $\Delta J \neq 0$ , the problem maps onto a biased random-field Ising model. In the case  $\Delta J > 0$ , horizontal stripes are preferred over vertical ones. Minority (vertical stripe) domains have a finite maximum size that decreases with increasing  $\Delta J$  [21]. At low temperatures, we thus expect the system to consist of finite-size vertical-stripe domains embedded in the bulk featuring horizontal stripes.

The domains of the two-dimensional random-field Ising model were further investigated by Seppälä *et al.* [43] and by Stevenson and Weigel [44]. They demonstrated that the domain structure in the unbiased case on length scales larger than  $L_0$  resembles the fractal cluster structure of a critical percolation problem, at least for sufficiently weak random fields (i.e., sufficiently large  $L_0$ ). Increasing bias ( $\Delta J > 0$ ) drives the domain pattern away from percolation criticality, and a massive spanning cluster of the majority stripes forms. This transition in the domain structure is governed by the usual two-dimensional classical percolation exponents.

### D. Magnetic phase transition

The random-field disorder in the diluted  $J_1$ - $J_2$  model locally breaks the  $C_4$  rotation symmetry of the square lattice. However, it does not break the  $Z_2$  Ising spin symmetry. This leaves open the possibility of a magnetic phase transition into a long-range ordered low-temperature phase that spontaneously breaks this remaining  $Z_2$  symmetry [45]. This phase transition, if any, has to occur on the background of the stripe domain pattern discussed in Sec. II C.

In the absence of a global anisotropy (i.e., for  $\Delta J = 0$ ), the magnetic phase transition is impossible because the domain structure resembles critical percolation. This implies that neither horizontal nor vertical domains form a massive cluster that covers a finite fraction of the lattice sites and can support long-range magnetic order. This conclusion agrees with the Monte Carlo results of Ref. [36].

In the presence of a global anisotropy, in contrast, the majority stripes (horizontal stripes for  $\Delta J > 0$ ) form a massive infinite (spanning) cluster. The Ising spins on this cluster can therefore spontaneously break the  $Z_2$  Ising symmetry and develop long-range order. To estimate the critical temperature  $T_c$  of the magnetic transition as function of the global anisotropy  $\Delta J$ , we recall that the critical temperature of a diluted Ising model close to the percolation threshold  $p_c$  varies as  $T_c \sim 1/|\ln(p - p_c)|$  with the distance  $p - p_c$  from the threshold (see, e.g., [46,47]). In our  $J_1$ - $J_2$  model (2), the distance of the stripe domain pattern from percolation criticality is controlled by  $\Delta J$ . We therefore expect the transition temperature into the stripe phase to vary as

$$T_c \sim 1/|\ln(\text{const } \Delta J)|. \quad (5)$$

In addition to random-field disorder, the vacancies also create random-mass disorder, which is known to prevent first-order phase transitions in two dimensions [2–4]. We thus expect the transition into the stripe phase to be continuous. On symmetry grounds, its critical behavior should belong to the two-dimensional disordered Ising universality class as it spontaneously breaks the remaining  $Z_2$  symmetry. This is a particularly interesting universality class because the clean two-dimensional Ising correlation length exponent takes the

value  $\nu = 1$ , which makes it marginal with respect to the Harris criterion [5]  $d\nu > 2$ . Perturbative renormalization-group studies [48–50] predict that the critical behavior of the disordered Ising model is controlled by the clean Ising fixed point. Disorder, which is a marginally irrelevant operator, gives rise to universal logarithmic corrections to scaling. Early computer simulations [51–53], in contrast, found nonuniversal critical exponents that vary continuously with disorder strength. More recent large-scale simulations strongly support the logarithmic-corrections scenario (see Ref. [54] and references therein).

### III. MONTE CARLO SIMULATIONS

In order to gain a quantitative understanding of the interplay between the random fields and the global anisotropy in the  $J_1$ - $J_2$  model, we perform extensive Monte Carlo simulations of the Hamiltonian (2). As we are interested in the fate of the stripe low-temperature phase, we fix the interaction energies at the values  $J_1 = -J_2 = 1$  for which the undiluted isotropic system enters the stripe phase at a temperature of about 2.08 [40]. The dilution is fixed at  $p = 0.25$ . This relatively strong disorder leads to moderate domain sizes that actually fit into the sample sizes we are able to simulate. The global interaction anisotropy  $\Delta J$  is varied between 0 and 0.2.

In the parameter region  $J_1 > 0, J_2 < 0$ , the interactions of the  $J_1$ - $J_2$  model are frustrated. Therefore, cluster algorithms such as the Wolff [55] and Swendsen-Wang [56] algorithms do not improve the efficiency of the simulations [57]. We therefore combine conventional single-spin-flip Metropolis updates [58] with “corner” updates that exchange the two spins on the diagonal corners of a  $2 \times 2$  plaquette of sites. These corner updates locally turn horizontal stripes into vertical ones and vice versa. Specifically, a full Monte Carlo sweep consists of a Metropolis sweep over the full lattice followed by two corner sweeps (one attempting to exchange the top-right and bottom-left sites of each plaquette, the other doing the same for the top-left and bottom-right sites).

As both Monte Carlo moves are local, equilibration is slow, and the problem is further exacerbated by the random-field effects at nonzero dilution. This is illustrated in Fig. 4, which shows how the energy approaches its equilibrium value (for a prototypical set of parameters). The data demonstrate that the relaxation is slower than exponential, it approximately follows a power law over at least two orders of magnitude in Monte Carlo time.

Consequently, long equilibration periods are required in the simulations, as well as long measurement periods to ensure that the measurements do not remain correlated over the simulation run. This severely limits the system sizes we can study. We employ equilibration periods ranging from 30 000 full sweeps for the smallest systems (linear size  $L = 16$ ) to  $10^6$  sweeps for the largest systems studied ( $L = 192$ ). The corresponding measurement periods range from 30 000 to  $2 \times 10^6$  full sweeps, with a measurement taken after each sweep. We also change the temperature in small steps and use the final spin configuration for one temperature as the initial configuration for the next. To check whether the observables truly reach their equilibrium values (within the statistical errors), we compare the results of runs with “hot” starts (spins

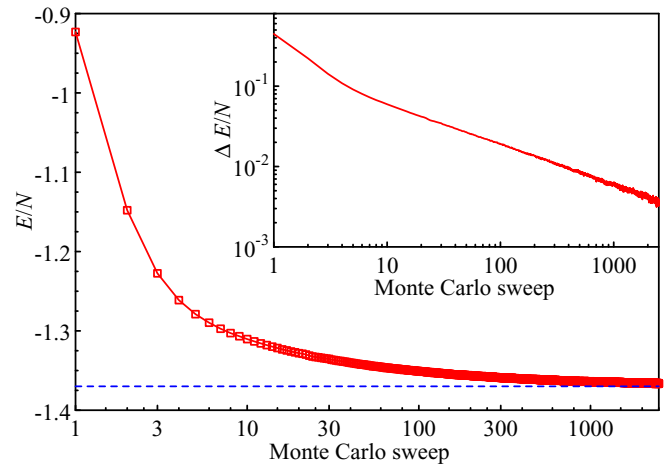


FIG. 4. Energy per site  $E/N$  vs Monte Carlo sweep for a system of linear size  $L = 96$ ,  $\Delta J = 0$ , and temperature  $T = 1.15$ . The data are averages over 3000 runs, each with a different disorder configuration. The simulations start from a random configuration of spins (hot start). The dashed line marks the equilibrium value of  $E/N$ . Inset: Log-log plot of the deviation  $\Delta E$  from the equilibrium value vs Monte Carlo sweep.

have independent random values initially) and “cold” starts (spins are in perfect stripe state initially). An example of such a comparison is shown in Fig. 5. All data are averaged over 3000 to 100 000 disorder (vacancy) configurations, depending on system size and temperature range.

During the simulations, we compute a number of observables including the total energy per site  $[\langle e \rangle]_{\text{dis}}$  and the specific heat  $C = (N/T^2)[\langle e^2 \rangle - \langle e \rangle^2]_{\text{dis}}$ . Here,  $e = E/N$  stands for an individual energy measurement,  $\langle \dots \rangle$  is the canonical ther-

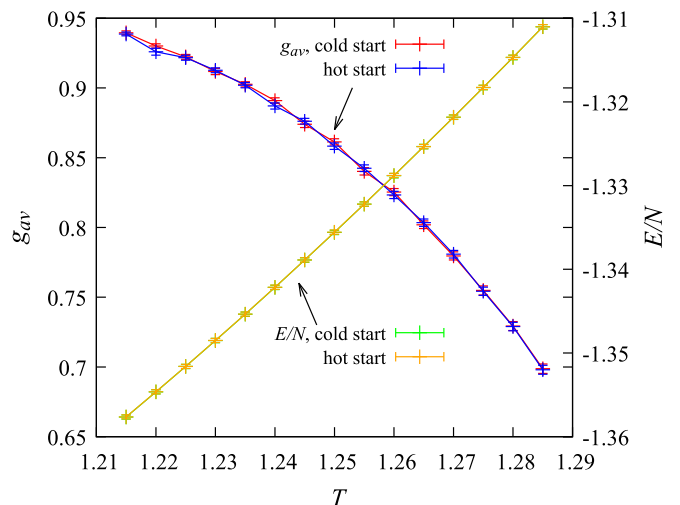


FIG. 5. Comparison of simulations with hot starts (random initial spin configuration, run starts at highest temperature) and cold starts (spins initially in perfect stripe state, run starts at lowest temperature). Shown are the average Binder cumulant  $g_{\text{av}}$  and the total energy per site  $E/N$  as function of temperature  $T$  for a system with  $L = 96$ ,  $\Delta J = 0.01$ . The data are averages over 5000 runs, each with a different disorder configuration, using  $3 \times 10^5$  equilibration sweeps and  $4 \times 10^5$  measurement sweeps.

modynamic average (which is approximated by the Monte Carlo average) and  $[\dots]_{\text{dis}}$  is the average over the disorder configurations. We also calculate the two-component stripe order parameter  $\psi = (\psi_h, \psi_v)$  with

$$\psi_h = \frac{1}{N} \sum_i (-1)^{y_i} \epsilon_i S_i, \quad \psi_v = \frac{1}{N} \sum_i (-1)^{x_i} \epsilon_i S_i. \quad (6)$$

Here, the indices  $h$  and  $v$  denote horizontal and vertical stripe order, respectively, and  $x_i$  and  $y_i$  are the (integer) coordinates of site  $i$ . The corresponding stripe susceptibility reads  $\chi_s = (N/T)[\langle |\psi|^2 \rangle - \langle |\psi|^2 \rangle_{\text{dis}}]$ . Dimensionless observables are particularly useful for finding the phase transition temperature and analyzing the critical behavior. We therefore also determine the average and global Binder cumulants

$$g_{\text{av}} = \left[ 2 - \frac{\langle |\psi|^4 \rangle}{\langle |\psi|^2 \rangle^2} \right]_{\text{dis}}, \quad g_{\text{gl}} = 2 - \frac{[\langle |\psi|^4 \rangle]_{\text{dis}}}{[\langle |\psi|^2 \rangle]_{\text{dis}}^2}. \quad (7)$$

With increasing system size, these Binder cumulants are expected to approach the values 0 in the disordered phase and 1 in the stripe-ordered phase, and curves of the Binder cumulants vs temperature for different system sizes cross at the phase transition temperature.  $g_{\text{av}}$  and  $g_{\text{gl}}$  capture similar information and are expected to have identical scaling behaviors, but they differ in how the disorder average is performed. For the average Binder cumulant  $g_{\text{av}}$ , an individual Binder cumulant is computed for each disorder configuration. These individual values are then averaged to yield  $g_{\text{av}}$ . To obtain the global Binder cumulant  $g_{\text{gl}}$ , in contrast, the second and fourth moment of the stripe order parameter are averaged over the disorder configurations, and the cumulant is then constructed from these disorder-averaged values. In the present paper, we employ the average Binder cumulant for most of the analysis because it shows weaker corrections to scaling at the transition into the stripe phase.

## IV. RESULTS

### A. Isotropic interactions, $\Delta J = 0$

To test our simulation and data analysis techniques, we first consider  $\Delta J = 0$ , i.e., equal exchange interactions  $J_{1h}$  and  $J_{1v}$  in the horizontal and vertical directions, respectively. This case can be compared with Ref. [36] and serves as the reference case for studying the effects of anisotropic interactions.

Figure 6 presents the Monte Carlo simulation results for the average stripe Binder cumulant  $g_{\text{av}}$  as a function of temperature  $T$  for several system sizes  $L$  at dilution  $p = 1/4$  and  $J_1 = -J_2 = 1$ . The curves for different  $L$  do not cross, instead  $g_{\text{av}}$  approaches zero with increasing  $L$ . The global Binder cumulant  $g_{\text{gl}}$  behaves analogously [59]. This implies that there is no phase transition, and the system does not enter a long-range ordered stripe phase. This agrees with the expectation of domain formation according to the Imry-Ma argument discussed in Sec. II C and with the results of Ref. [36].

The domains can be seen explicitly in a snapshot of the local nematic order parameter  $\eta_i$  in Fig. 7. It is defined via a sum over all bonds from site  $i$  to its nearest neighbors,  $\eta_i = \sum_j' \epsilon_i \epsilon_j S_i S_j f_{ij}$  where  $f_{ij} = 1$  for horizontal bonds and  $-1$  for vertical bonds. (This means that  $\eta_i = 4$  for perfect horizontal stripe order and  $-4$  for perfect vertical stripe order).

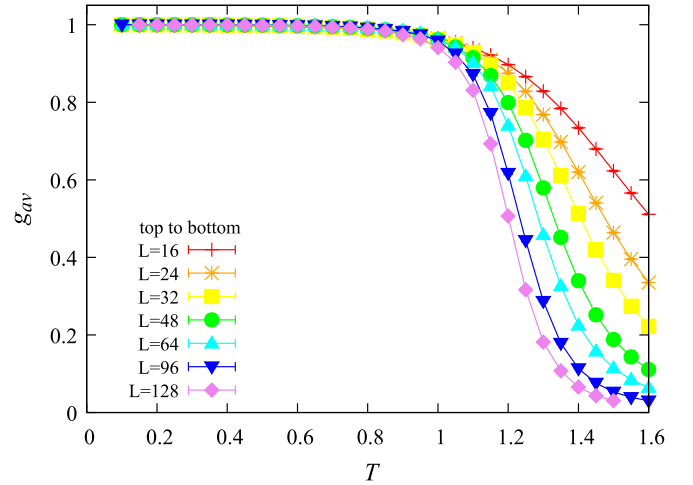


FIG. 6. Average Binder cumulant  $g_{\text{av}}$  vs temperature  $T$  for isotropic interactions  $\Delta J = 0$  and several system sizes  $L$ .  $p = 1/4$ ,  $J_1 = -J_2 = 1$ . The data are averages over 3000 to 5000 disorder configurations. The resulting statistical errors are smaller than the symbol size.

The figure indicates that horizontal and vertical stripes are equally likely for  $\Delta J = 0$ , as expected in the isotropic case. It also suggests a breakup length  $L_0$  in the range between about 50 and 100 lattice constants. It is interesting to compare this estimate with the random-field Ising model result (4). Using the values  $A \approx 6.1$  and  $c \approx 1.9$  found numerically by Seppälä *et al.* [43], Eq. (4) yields a breakup length of about  $2 \times 10^7$  for  $p = 1/4$ , much larger than the length identified in Fig. 7. We believe that this stems from the fact that the domain wall energy in the diluted system is significantly smaller than the value  $2|J_2|$  per unit cell in the undiluted system because the domain wall can make use of the vacancies to reduce the number of unfulfilled bonds. In fact, assuming that the vacancies reduce the domain wall energy by a factor of 2 to 3, Eq. (4) yields breakup length values comparable to the sizes seen in Fig. 7.

Thus, the vacancies play a complex role in the destruction of the stripe order: They generate random fields, they renormalize the domain wall energy, and they create random-mass disorder.

### B. Anisotropic interactions, $\Delta J > 0$

We now turn to the main topic of this paper, the effects of a weak global interaction anisotropy  $\Delta J$ . To this end, we perform Monte Carlo simulations for  $\Delta J = 0.002, 0.005, 0.01, 0.02, 0.05, 0.1, \text{ and } 0.2$ . Snapshots of the resulting local nematic order parameter  $\eta_i$  at low temperatures are presented in Fig. 7 for a few characteristic  $\Delta J$  values. As expected from the discussion in Sec. II C, the snapshots show that horizontal stripes proliferate with increasing  $\Delta J$  and form an infinite spanning cluster while vertical stripes are restricted to finite-size clusters. Already at  $\Delta J = 0.05$ , vertical stripe domains have essentially vanished.

To investigate whether or not the systems feature a phase transition into a long-range ordered stripe phase, we analyze the average Binder cumulant  $g_{\text{av}}$ . For all  $\Delta J \geq 0.005$ , we find that the stripe Binder cumulant curves for different sys-

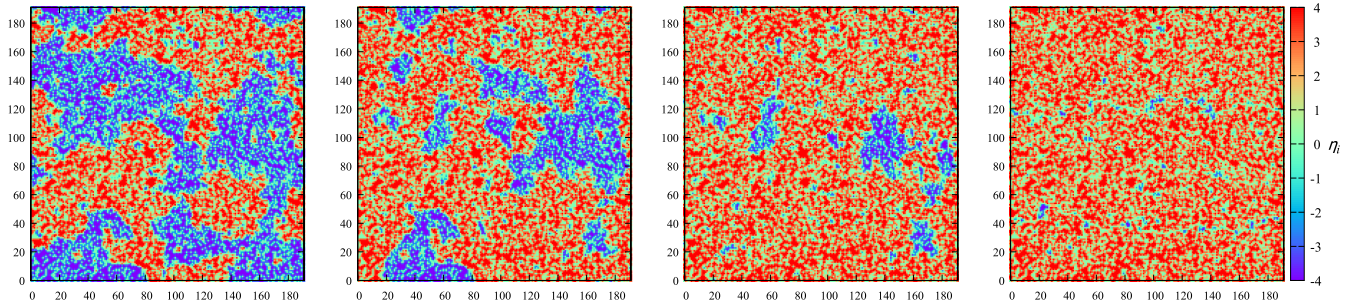


FIG. 7. Snapshots of the local nematic order parameter  $\eta_i$  of one particular disorder configuration for several anisotropies:  $\Delta J = 0, 0.002, 0.01, 0.05$  (left to right). The data are taken a temperature  $T = 0.1$  reached via simulated annealing from high temperatures.  $L = 192, p = 1/4, J_1 = -J_2 = 1$ .

tem sizes  $L$  cross at a nonzero temperature, indicating the existence of the phase transition. Examples of the average Binder cumulant data are presented in Figs. 8 and 9. The global Binder cumulant behaves analogously. The curves for  $\Delta J = 0.2$  (Fig. 8) display a nearly perfect crossing for all considered system sizes, demonstrating that corrections to scaling are weak. For  $\Delta J = 0.005$  (Fig. 9), in contrast, the curves for smaller system sizes ( $L < 64$ ) do not cross and resemble the isotropic  $\Delta J = 0$  case. The curves for larger systems cross but the crossing temperature of consecutive curves shifts systematically to higher values with increasing  $L$ . This indicates that the data for the studied system sizes have not quite reached the asymptotic critical regime.

The fact that the Binder cumulant curves for smaller sizes do not cross for weak anisotropy is readily understood by comparing the random field energy at a given system size with the energy gain for horizontal stripes due to  $\Delta J$ . According to Eq. (3), the typical energy gain due to aligning a domain of size  $L$  with the local random fields is  $h_{\text{eff}}L = \sqrt{2}pJ_1L$  whereas the anisotropy favors horizontal stripes by the energy  $\Delta JL^2$ . A weak anisotropy can thus only suppress vertical domains of sizes larger than  $L_{\Delta J} \approx \sqrt{2}pJ_1/\Delta J$  [60]. For  $\Delta J = 0.005$ ,

this estimate gives  $L_{\Delta J} \approx 70$  in agreement with the observation that crossings start to appear for  $L \geq 64$ . For  $\Delta J = 0.002$ , the smallest domain that the anisotropy can flip has a size of about  $L \approx 175$ . As our system sizes are restricted to  $L \leq 192$ , this explains why we do not observe clear crossings of the Binder cumulant curves for  $\Delta J = 0.002$ . In other words, identifying the phase transition for  $\Delta J \leq 0.002$  requires simulations of significantly larger systems.

We now analyze how the transition temperature  $T_c$  into the stripe-ordered phase varies with the interaction anisotropy  $\Delta J$ . To this end, we determine the crossing temperature for each  $\Delta J$  value. This is unambiguous for the larger  $\Delta J$  for which the crossing is “sharp”, i.e., the curves all cross at the same temperature within their statistical errors. For the smaller  $\Delta J$ , where the crossing shifts with increasing  $L$ , we estimate  $T_c$  from the crossing of the largest two system sizes [61].

Figure 10 presents the resulting dependence of  $T_c$  on  $\Delta J$ . The data show that  $T_c$  rises very rapidly as  $\Delta J$  increases from zero implying that a small global anisotropy is sufficient to stabilize a robust stripe phase. The figure also demonstrates

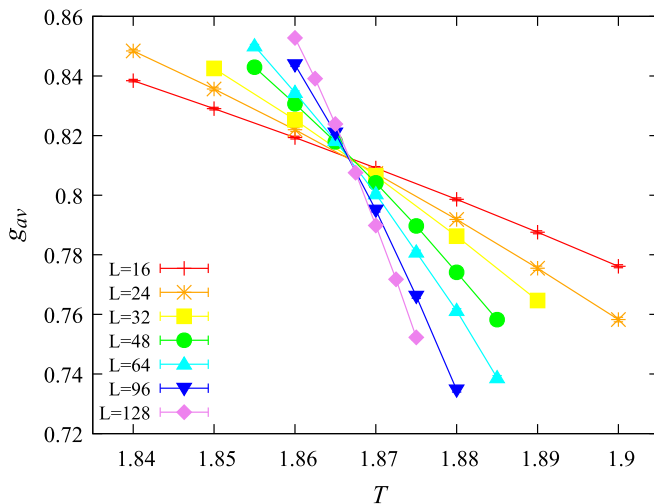


FIG. 8. Average Binder cumulant  $g_{\text{av}}$  vs temperature  $T$  for anisotropic interactions with  $\Delta J = 0.2$  and several system sizes  $L$ .  $p = 1/4, J_1 = -J_2 = 1$ . The data are averages over 30 000 to 100 000 disorder configurations. The resulting statistical errors are much smaller than the symbol size.

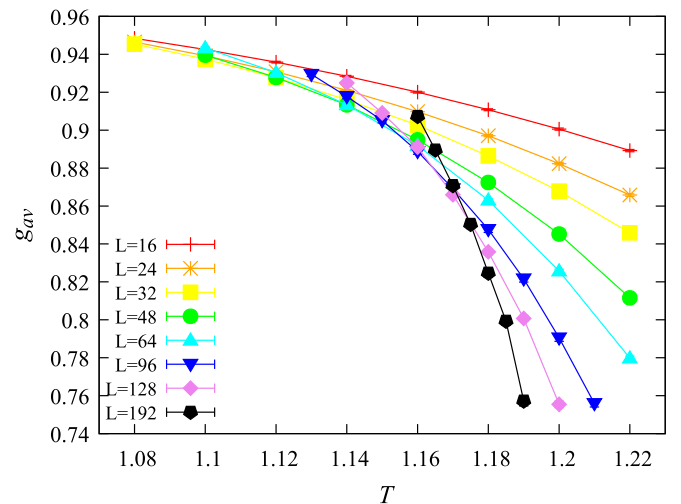


FIG. 9. Average Binder cumulant  $g_{\text{av}}$  vs temperature  $T$  for anisotropic interactions with  $\Delta J = 0.005$  and several system sizes  $L$ .  $p = 1/4, J_1 = -J_2 = 1$ . The data are averages over 10 000 to 20 000 disorder configurations. The statistical errors are smaller than the symbol size.

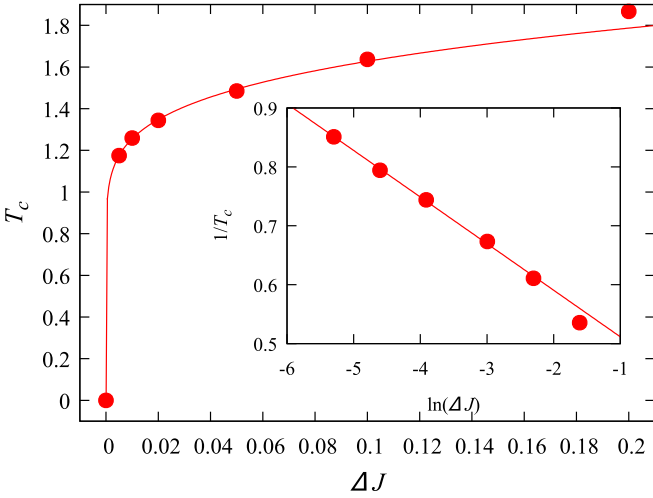


FIG. 10. Transition temperature  $T_c$  into the long-range stripe ordered phase vs interaction anisotropy  $\Delta J$  for  $p = 1/4, J_1 = -J_2 = 1$ . The solid line is a fit of the data for  $\Delta J < 0.2$  with the logarithmic dependence (5) yielding  $1/T_c = -0.0791 \ln(\Delta J) + 0.432$ . Inset: Data replotted as  $1/T_c$  vs  $\ln \Delta J$  such that (5) leads to a straight line.

that  $T_c$  follows the logarithmic dependence (5) on  $\Delta J$  predicted in Sec. IID for all  $\Delta J \leq 0.1$ .

It is interesting to compare the critical temperatures in Fig. 10 with the corresponding value  $T_{c0} \approx 2.08$  [40] for the undiluted isotropic system at the same parameter values ( $J_1 = -J_2 = 1$ ). Our simulations show that a weak anisotropy of  $\Delta J = 0.005$  already produces a  $T_c$  of more than half of the undiluted value. Moreover, a large part of the reduction can be attributed to the random-mass effects of the dilution in our system and not the random-field physics. Thus, a better comparison may be the diluted system with anticorrelated impurities studied in Ref. [36]. In that system, the random-field physics is completely eliminated by the vacancy anticorrelations. Its critical temperature of  $T_c \approx 1.17$  (for  $p = 1/4$  and  $J_1 = -J_2 = 1$ ) is comparable to the critical temperatures in Fig. 10 for anisotropies  $\Delta J$  that have largely suppressed the effects of the random-field disorder.

### C. Critical behavior

According to the discussion in Sec. IID, we expect the transition into the long-range stripe-ordered phase to be continuous and to belong to the two-dimensional disordered Ising universality class. A perturbative renormalization group approach [48–50] predicts its critical behavior to be controlled by the clean Ising fixed point while the disorder gives rise to universal logarithmic corrections to scaling. This leads to the following finite-size scaling behavior [62–64]. The specific heat at the critical temperature diverges as

$$C \sim \ln \ln L \quad (8)$$

with system size  $L$ . The order parameter and its susceptibility at  $T_c$  behave as

$$\psi \sim L^{-\beta/\nu} [1 + O(1/\ln L)], \quad (9)$$

$$\chi_s \sim L^{\gamma/\nu} [1 + O(1/\ln L)], \quad (10)$$

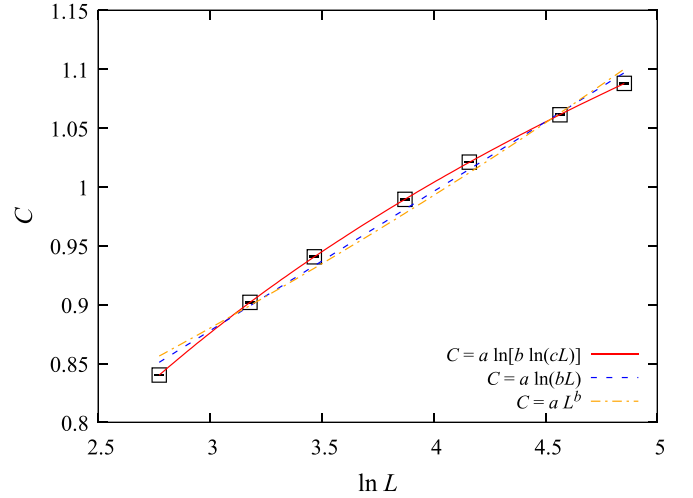


FIG. 11. Semilog plot of the specific heat  $C$  vs system size  $L$  at the critical temperature  $T_c = 1.8670$  for  $\Delta J = 0.2, J_1 = -J_2 = 1, p = 1/4$ . The data are averages over 30,000 to 100,000 disorder configurations. The resulting statistical errors are much smaller than the symbol size. The solid line represents a fit with  $C = a \ln[b \ln(cL)]$ . The dashed and dash-dotted lines represent a simple logarithmic fit  $C = a \ln(bL)$  and a power-law fit  $C = a L^b$ , respectively.

with  $\beta/\nu = 1/8$  and  $\gamma/\nu = 7/4$  as in the clean two-dimensional Ising model. Any quantity  $R$  of scale dimension zero (such as the Binder cumulants  $g_{av}$  and  $g_{gl}$ ) and its temperature derivative scale as

$$R = R^* + O(1/\ln L), \quad (11)$$

$$dR/dT \sim L^{1/\nu} (\ln L)^{-1/2} [1 + O(1/\ln L)] \quad (12)$$

with the clean Ising value  $\nu = 1$ .

Identifying logarithmic corrections in numerical simulations and distinguishing them from power laws with small exponents requires high-quality data over a significant system-size range. Here, we therefore focus on  $\Delta J = 0.2$  for which the system reaches the asymptotic critical regime for smaller  $L$  than for weaker anisotropies (see Figs. 8 and 9). We also simulate more disorder configurations for  $\Delta J = 0.2$  than for the other  $\Delta J$  to further reduce the statistical errors.

To test the theoretical predictions (8) to (12), we analyze the system-size dependence of  $C$ ,  $\psi$ ,  $\chi_s$ , and  $dg_{av}/dT$  at the critical temperature  $T_c = 1.8670$ . (We use polynomial interpolations in  $T$  to determine these values from the simulation data.) Figure 11 presents a semilogarithmic plot of the specific heat  $C$  vs the system size  $L$ . The figure clearly shows that the specific heat grows slower than logarithmic with  $L$ . It can be fitted well with the double-logarithmic form  $a \ln[b \ln(cL)]$  suggested by Eq. (8), giving a reduced error sum  $\bar{\chi}^2$  below unity [65]. In contrast, both a simple logarithmic fit  $C = a \ln(bL)$  and a power-law fit  $C = a L^b$  lead to unacceptably large reduced  $\bar{\chi}^2$  values of about 800 and 1600, respectively.

To test the predicted behavior (10) of the stripe susceptibility, we divide out the clean Ising power law and plot  $\chi_s L^{-7/4}$  vs  $L$  in Fig. 12. The figure demonstrates that  $\chi_s L^{-7/4}$

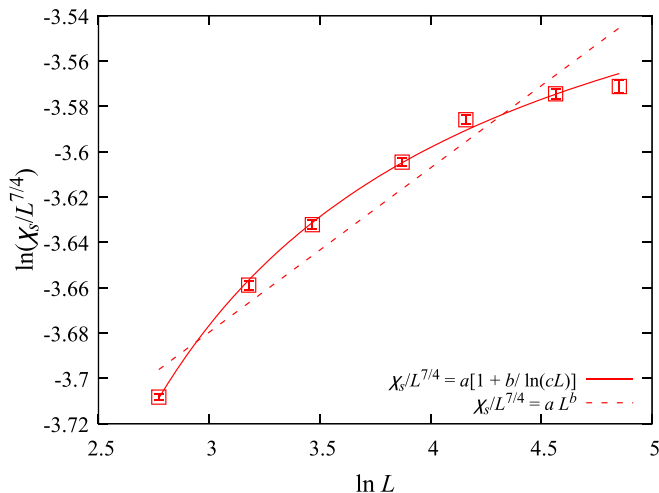


FIG. 12. Double logarithmic plot of  $\chi_s L^{-7/4}$  vs system size  $L$  at the critical temperature  $T_c = 1.8670$  for  $\Delta J = 0.2$ ,  $J_1 = -J_2 = 1$ ,  $p = 1/4$ . The data are averages over 30 000 to 100 000 disorder configurations. The solid line represents a fit with  $a[1 + b/\ln(cL)]$ . The dashed line represents a simple power-law fit with the functional form  $aL^b$ .

increases more slowly than a power law with  $L$ . The data can be fitted reasonably well with the form  $a[1 + b/\ln(cL)]$ , yielding a reduced error sum of  $\bar{\chi}^2 \approx 2.9$ . (The reduced error sum drops to about 1.3 if the smallest system size,  $L = 16$ , is discarded.) A power-law fit produces a unacceptably large  $\bar{\chi}^2$  of about 60. The stripe order parameter can be treated analogously, i.e., by analyzing  $\psi L^{1/8}$ . However, the corrections to the clean Ising behavior for  $\psi$  are much weaker than those for  $\chi_s$ , they only lead to a relative variation of  $\psi L^{1/8}$  by about 1% over the size range from  $L = 16$  to 128. Within the given statistical errors, both (9) and a power law  $\psi \sim L^{-\beta/\nu}$  with  $\beta/\nu \approx 0.120$  fit the data.

Finally, we analyze the system-size dependence of the slopes  $dg_{av}/dT$  of the Binder cumulant curves at criticality. Within the statistical errors of our data and the uncertainty of  $T_c$ , we cannot discriminate between Eq. (12) and simple power law  $dg_{av}/dT \sim L^{1/\nu}$  (which gives  $\nu \approx 1.12$ ). Both functional forms fit the data reasonably well.

Taken together, the analyses of  $C$ ,  $\psi$ ,  $\chi_s$ , and  $dg_{av}/dT$  provide strong evidence for the critical behavior to belong to the two-dimensional disordered Ising universality class, characterized by the clean Ising exponents with universal logarithmic corrections. To confirm that this behavior also holds for smaller anisotropies, we have studied the system size dependence of the specific heat at criticality for the other simulated  $\Delta J$  values. For all  $\Delta J > 0.01$ , the specific heat data can be fitted well with the double logarithmic form (8), giving reduced error sums around unity. Even for the smallest  $\Delta J = 0.01$  and 0.005, the double logarithmic form fits much better than a simple logarithmic dependence or a power law. However, the fit quality is noticeably worse ( $\bar{\chi}^2 \approx 3$  and 6, respectively). This can be attributed to the fact that the systems with  $\Delta J \leq 0.01$  have not reached the asymptotic critical regime in the size range  $L = 16$  to 128 (see Fig. 9).

## V. CONCLUSION

To summarize, we have investigated the combined influence of spinless impurities and a spatial interaction anisotropy on the low-temperature stripe phase in the frustrated square-lattice  $J_1$ - $J_2$  Ising model. The impurities reduce the effective interaction strength and thus create random-mass disorder. They also locally break the  $C_4$  rotation symmetry of the lattice, and thus create effective random fields coupling to the nematic order parameter that distinguishes the two possible stripe directions. In the absence of a global anisotropy, these random fields destroy the stripe phase via domain formation.

A global interaction anisotropy that explicitly breaks the  $C_4$  lattice symmetry competes with the random fields and restores the stripe phase at sufficiently low temperatures. By combining percolation theory and results about the domain structure of a biased random-field Ising model, we have predicted that the transition temperature  $T_c$  into the stripe phase varies as  $T_c \sim 1/|\ln(\Delta J)|$  with the interaction anisotropy  $\Delta J$ . This means very small  $\Delta J$  are sufficient to restore a robust stripe phase.

We have also studied the resulting phase transition into the stripe phase. Our Monte Carlo results provide strong numerical evidence for the transition to be continuous and to belong to the disordered two-dimensional Ising universality class, which is characterized by the clean Ising exponents and universal logarithmic corrections.

Our explicit calculations have implemented the global anisotropy via a difference between the nearest-neighbor interactions in the two lattice directions. Other sources of global anisotropies that break the symmetry between the two stripe directions are expected to have analogous effects. For example, a global anisotropy in the impurity distribution that favors impurity pairs on, say, horizontal nearest-neighbor sites over pairs on vertical nearest-neighbor sites introduces a bias into the random field distribution. Horizontal stripe domains thus proliferate and form a massive spanning cluster, just as in our case.

Let us also comment on the possibility of a nematic phase. In the absence of a global anisotropy, ( $\Delta J = 0$ ), the phase transition between the paramagnetic high-temperature phase and the stripe low-temperature phase, if any, could in principle split into two separate transitions, the first breaking the  $C_4$  lattice symmetry, producing nematic order, and the second breaking the Ising spin symmetry. In the clean  $J_1$ - $J_2$  Ising model, a nematic phase has not been observed, and same holds for the diluted model studied in Ref. [36] in which the random-field physics is suppressed by impurity anticorrelations. The  $J_1$ - $J_2$  Heisenberg model, in contrast, hosts a nematic phase [66]. We emphasize that a nematic phase transition cannot occur in principle in the presence of a nonzero anisotropy  $\Delta J \neq 0$ . The anisotropy breaks the  $C_4$  lattice symmetry explicitly, spontaneous breaking of this symmetry is thus impossible [67].

Our results have demonstrated that the random-field effects generated by spinless impurities (and, by analogy, bond dilution or other types of quenched randomness) on an order parameter that breaks a real-space symmetry are very sensitive to weak global spatial anisotropies. This may complicate the experimental observation of the random-field physics, for example if the samples feature residual strain. A systematic



variation of the anisotropy to test the predictions of the present paper may be achieved, e.g., by applying uniaxial pressure.

We note that the interplay and feedback between the random-field induced domain formation and the magnetic degrees of freedom leads to enhanced fluctuations and slow dynamics even in the absence of a global anisotropy, as was recently demonstrated by mapping the  $J_1$ - $J_2$  Hamiltonian on an Ashkin-Teller model in a random Baxter field [68].

It is interesting to compare our results to those for the square-lattice  $J_1$ - $J_2$  Heisenberg model. Even though magnetic long-range order at nonzero temperatures is impossible in the Heisenberg case due to the Mermin-Wagner theorem [69], the clean  $J_1$ - $J_2$  Heisenberg model features vestigial nematic order [66] associated with the unrealized stripe phase (for  $|J_2| > J_1/2$ ). Fyodorov and Shender [32] argued that random bond dilution creates random fields for the nematic order just as in the Ising case, destroying the nematic phase. Recently, Miranda *et al.* [20] demonstrated that this conclusion holds generically for both bond disorder and site vacancies. As a result, the system is a nontrivial paramagnet for nonzero temperatures, and a spin-vortex-crystal glass for zero temperature and weak disorder [20].

Impurity-induced random fields also emerge in three-dimensional frustrated magnets. For example, in XY

pyrochlore magnets, they have recently been shown to destroy long-range order beyond a critical disorder strength, leading to the formation of a cluster-glass state [37].

The use of strain to manipulate and “engineer” phases and properties of many-particle systems has recently attracted considerable attention. For instance, it was realized that strain can lift the degeneracy of the ground state manifold of a frustrated Heisenberg antiferromagnet on a Kagome lattice, tuning the system through a sequence of unconventional phases [70]. Our results can be understood as an example of using strain engineering to restore the stripe phase.

## ACKNOWLEDGMENTS

The work in Missouri has been supported in part by the National Science Foundation under Grants No. DMR-1828489 and No. OAC-1919789. The simulations were performed on the Pegasus and Foundry clusters at Missouri S&T. R.N. acknowledges funding from the Center for Quantum Information Theory in Matter and Spacetime, IIT Madras, and from the Department of Science and Technology, Govt. of India, under Grant No. DST/ICPS/QuST/Theme-3/2019/Q69. We also thank Rafael Fernandes and Joe Meese for helpful discussions.

- 
- [1] T. Vojta, *Ann. Rev. Condens. Mat. Phys.* **10**, 233 (2019).  
 [2] Y. Imry and M. Wortis, *Phys. Rev. B* **19**, 3580 (1979).  
 [3] K. Hui and A. N. Berker, *Phys. Rev. Lett.* **62**, 2507 (1989).  
 [4] M. Aizenman and J. Wehr, *Phys. Rev. Lett.* **62**, 2503 (1989).  
 [5] A. B. Harris, *J. Phys. C* **7**, 1671 (1974).  
 [6] D. S. Fisher, *Phys. Rev. Lett.* **69**, 534 (1992); *Phys. Rev. B* **51**, 6411 (1995).  
 [7] O. Motrunich, S. C. Mau, D. A. Huse, and D. S. Fisher, *Phys. Rev. B* **61**, 1160 (2000).  
 [8] J. A. Hoyos, C. Kotabage, and T. Vojta, *Phys. Rev. Lett.* **99**, 230601 (2007); T. Vojta, C. Kotabage, and J. A. Hoyos, *Phys. Rev. B* **79**, 024401 (2009).  
 [9] T. Vojta, *Phys. Rev. Lett.* **90**, 107202 (2003); J. A. Hoyos and T. Vojta, *ibid.* **100**, 240601 (2008).  
 [10] R. B. Griffiths, *Phys. Rev. Lett.* **23**, 17 (1969).  
 [11] M. Thill and D. A. Huse, *Physica A* **214**, 321 (1995).  
 [12] H. Rieger and A. P. Young, *Phys. Rev. B* **54**, 3328 (1996); A. P. Young and H. Rieger, *ibid.* **53**, 8486 (1996).  
 [13] T. Vojta, *J. Phys. A* **39**, R143 (2006); *J. Low Temp. Phys.* **161**, 299 (2010).  
 [14] T. Vojta, *AIP Conf. Proc.* **1550**, 188 (2013).  
 [15] Y. Imry and S.-k. Ma, *Phys. Rev. Lett.* **35**, 1399 (1975).  
 [16] R. Harris, M. Plischke, and M. J. Zuckermann, *Phys. Rev. Lett.* **31**, 160 (1973).  
 [17] R. A. Pelcovits, E. Pytte, and J. Rudnick, *Phys. Rev. Lett.* **40**, 476 (1978).  
 [18] D. S. Fisher, *Phys. Rev. B* **31**, 7233 (1985).  
 [19] M. Dudka, R. Folk, and Y. Holovatch, *J. Magn. Magn. Mater.* **294**, 305 (2005).  
 [20] M. M. J. Miranda, I. C. Almeida, E. C. Andrade, and J. A. Hoyos, *Phys. Rev. B* **104**, 054201 (2021).  
 [21] K. Binder, *Z. Phys. B* **50**, 343 (1983).  
 [22] V. J. Emery, S. A. Kivelson, and J. M. Tranquada, *Pro. Nat. Acad. Sci. USA* **96**, 8814 (1999).  
 [23] S. A. Kivelson, I. P. Bindloss, E. Fradkin, V. Oganesyan, J. M. Tranquada, A. Kapitulnik, and C. Howald, *Rev. Mod. Phys.* **75**, 1201 (2003).  
 [24] M. Vojta, *Adv. Phys.* **58**, 699 (2009).  
 [25] E. Fradkin, S. A. Kivelson, M. J. Lawler, J. P. Eisenstein, and A. P. Mackenzie, *Ann. Rev. Condens. Mat. Phys.* **1**, 153 (2010).  
 [26] R. M. Fernandes, A. V. Chubukov, and J. Schmalian, *Nat. Phys.* **10**, 97 (2014).  
 [27] E. Fradkin, S. A. Kivelson, and J. M. Tranquada, *Rev. Mod. Phys.* **87**, 457 (2015).  
 [28] N. Read and S. Sachdev, *Phys. Rev. Lett.* **62**, 1694 (1989).  
 [29] M. Mambri, A. Läuchli, D. Poilblanc, and F. Mila, *Phys. Rev. B* **74**, 144422 (2006).  
 [30] A. W. Sandvik, *Phys. Rev. Lett.* **98**, 227202 (2007).  
 [31] J. F. Fernandez, *Europhys. Lett. (EPL)* **5**, 129 (1988).  
 [32] Y. V. Fyodorov and E. F. Shender, *J. Phys. Condens. Mat.* **3**, 9123 (1991).  
 [33] E. W. Carlson, K. A. Dahmen, E. Fradkin, and S. A. Kivelson, *Phys. Rev. Lett.* **96**, 097003 (2006).  
 [34] Y. L. Loh, E. W. Carlson, and K. A. Dahmen, *Phys. Rev. B* **81**, 224207 (2010).  
 [35] L. Nie, G. Tarjus, and S. A. Kivelson, *Proc. Nat. Acad. Sci. USA* **111**, 7980 (2014).  
 [36] S. S. Kunwar, A. Sen, T. Vojta, and R. Narayanan, *Phys. Rev. B* **98**, 024206 (2018).  
 [37] E. C. Andrade, J. A. Hoyos, S. Rachel, and M. Vojta, *Phys. Rev. Lett.* **120**, 097204 (2018).  
 [38] S. Jin, A. Sen, and A. W. Sandvik, *Phys. Rev. Lett.* **108**, 045702 (2012).

- [39] S. Jin, A. Sen, W. Guo, and A. W. Sandvik, *Phys. Rev. B* **87**, 144406 (2013).
- [40] A. Kalz, A. Honecker, and M. Moliner, *Phys. Rev. B* **84**, 174407 (2011).
- [41] A. Kalz and A. Honecker, *Phys. Rev. B* **86**, 134410 (2012).
- [42] Note that the effective random-field strength is proportional to  $p$  rather than  $p^2$  as one might have naively expected because the probability for finding a vacancy pair is proportional to  $p^2$ .
- [43] E. T. Seppälä, V. Petäjä, and M. J. Alava, *Phys. Rev. E* **58**, R5217 (1998); E. T. Seppälä and M. J. Alava, *ibid.* **63**, 066109 (2001).
- [44] J. D. Stevenson and M. Weigel, *Europhys Lett.* **95**, 40001 (2011); *Comp. Phys. Commun.* **182**, 1879 (2011).
- [45] Note that situation differs from the random-field Ising model where the random fields completely break the order parameter symmetry.
- [46] D. Stauffer and A. Aharony, *Introduction to Percolation Theory* (CRC Press, Boca Raton, 1991).
- [47] J. Cardy, *Scaling and Renormalization in Statistical Physics* (Cambridge University Press, Cambridge, 1996).
- [48] V. S. Dotsenko and V. S. Dotsenko, *Adv. Phys.* **32**, 129 (1983).
- [49] B. N. Shalaev, *Fiz. Tverd. Tela (Leningrad)* **36**, 3002 (1984) [*Sov. Phys.–Solid State* **26**, 1811 (1984)].
- [50] R. Shankar, *Phys. Rev. Lett.* **58**, 2466 (1987).
- [51] M. Fähnle, T. Holey, and J. Eckert, *J. of Magn. Magn. Mater.* **104–107**, 195 (1992).
- [52] J.-K. Kim and A. Patrascioiu, *Phys. Rev. Lett.* **72**, 2785 (1994).
- [53] R. Kühn, *Phys. Rev. Lett.* **73**, 2268 (1994).
- [54] Q. Zhu, X. Wan, R. Narayanan, J. A. Hoyos, and T. Vojta, *Phys. Rev. B* **91**, 224201 (2015).
- [55] U. Wolff, *Phys. Rev. Lett.* **62**, 361 (1989).
- [56] R. H. Swendsen and J.-S. Wang, *Phys. Rev. Lett.* **58**, 86 (1987).
- [57] A. Kalz, A. Honecker, S. Fuchs, and T. Pruschke, *Eur. Phys. J. B* **65**, 533 (2008).
- [58] N. Metropolis, A. W. Rosenbluth, M. N. Rosenbluth, A. H. Teller, and E. Teller, *J. Chem. Phys.* **21**, 1087 (1953).
- [59] Note that  $g_{gl}$  and  $g_{av}$  have different low temperature limits.  $g_{av}$  approaches unity because the Binder cumulant of every single disorder realization reaches this value (assuming the ground state is unique up to symmetries).  $g_{gl}$ , in contrast, may approach a value below unity if different disorder realizations feature different order parameter values for  $T \rightarrow 0$ .
- [60] Note that this is a very rough estimate as it assumes compact domains, which only holds on scales below  $L_0$ . On larger length scales the cluster structure is fractal, see Sec. II C.
- [61] A systematic extrapolation of the crossing temperature to infinite system size, as performed, e.g., in Ref. [54], would require significantly lower statistical errors and is thus beyond our current computational capabilities.
- [62] G. Mazzeo and R. Kühn, *Phys. Rev. E* **60**, 3823 (1999).
- [63] M. Hasenbusch, F. Parisen Toldin, A. Pelissetto, and E. Vicari, *Phys. Rev. E* **78**, 011110 (2008).
- [64] R. Kenna and J. J. Ruiz-Lorenzo, *Phys. Rev. E* **78**, 031134 (2008).
- [65] For fitting  $n$  data points  $(x_i, y_i)$  to a function  $f(x)$  containing  $q$  fit parameters, the reduced error sum is defined as
- $$\bar{\chi}^2 = \frac{1}{n - q} \sum_i \frac{(y_i - f(x_i))^2}{\sigma_i^2} \quad (14)$$
- where  $\sigma_i^2$  is the variance of  $y_i$ . The fits are considered to be of good quality if  $\bar{\chi}^2 \lesssim 2$ .
- [66] P. Chandra, P. Coleman, and A. I. Larkin, *Phys. Rev. Lett.* **64**, 88 (1990).
- [67] This argument does not preclude more complicated scenarios such as a meta-nematic transition in analogy to a meta-magnetic transition in a ferromagnet.
- [68] W. J. Meese, T. Vojta, and R. M. Fernandes, [arXiv:2112.05769](https://arxiv.org/abs/2112.05769).
- [69] N. D. Mermin and H. Wagner, *Phys. Rev. Lett.* **17**, 1133 (1966).
- [70] M. M. Nayga and M. Vojta, [arXiv:2107.14249](https://arxiv.org/abs/2107.14249).